Available online at www.sciencedirect.com

SciVerse ScienceDirect

Ceramics International 39 (2013) 5309–5316

CERAMICS INTERNATIONAL

www.elsevier.com/locate/ceramint

Viscosity measurement of gelcasting slurry during in-situ gelation by a micro X-ray CT scan system

Shuichi Iwata[a,*], Tomoaki Kato[b], Ruben L. Menchavez[b,c], Masayoshi Fuji[b], Hideki Mori[a], Yumiko Yoshitake[d], Yusuke Yamada[a], Yasuhiro Saiki[a]

[a]*Department of Chemical Engineering, Nagoya Institute of Technology, Gokiso, Showa, Nagoya 466–8555, Japan*
[b]*Advanced Ceramics Research Center, Nagoya Institute of Technology, 3-101-1, Honmachi, Tajimi, Gifu 507-0033, Japan*
[c]*Ceramics and Metallurgical Department, College of Engineering, MSU-Iligan Institute of Technology, Tibanga, Iligan City 9200, Philippines*
[d]*Physics Course, Division of Science, School of Science and Engineering, Tokyo Denki University, Hatoyama-cho, Hiki-gun Saitama, 350-0394, Japan*

Received 29 October 2012; received in revised form 10 December 2012; accepted 10 December 2012
Available online 20 December 2012

Abstract

This paper reports the use of a micro X-ray CT scan system to measure the viscosity increase during in-situ gelation of a gelcasting slurry. Three small steel balls were dropped in the slurry at a desired time interval after the addition of the gelling agent, while being monitored by the CT scan system. It was determined that the plot of the logarithm of the calculated viscosities based on the settling velocity of the falling ball versus the gelation time can be classified into three regions with increasing slopes. The first region is designated as the idle time during which the gelcasting slurry can be further processed and cast into a mold. The second region is the onset of gelation during which the polymer networks start to form with a gradual increase in the viscosity, whereas the third region is attributed to the increased concentration of the polymerized networks as typified by the significant increase in the slurry viscosity. Moreover, the falling ball method was found to be more sensitive to detecting the onset of gel formation in the gelcasting slurry than stress-controlled rheometric analyses.

Keywords: Gelcasting; Gelation; Alumina slurry; Falling-ball viscometer

1. Introduction

The gelcasting process [1–3] is one of the promising methods for shaping a ceramic body, which employs an in-situ solidification technology for a slurry mixture through formations of polymerized network structures. The slurry mixture typically consists of a ceramic powder, dispersant, and a small amount of chemical agents. The slurry mixture is dispersed and cast into an impermeable mold, followed by in-situ polymerization of the chemical components promoted by chemical agents such as an initiator and catalysts. The gelled green body possesses a uniform particle packing that results in a homogeneous microstructure after high temperature treatment. One of the advantages of this method is the convenient manufacturing of a green body with a complex-shape and homogeneous particle compact. For example, Young et al. [2] reported application of the gelcasting process to the near-net shaping of a turbine rotor with a complex geometry. Moreover, some successful accounts of using gelcasting technology have been demonstrated by Janney et al. [4] and Niihara et al. [5].

The success of the gelcasting technology in shaping a ceramic body relies on the proper knowledge of the processing and gelation parameters of the gelcasting slurry. Among these gelcasting parameters, the gelation parameters, such as idle time, viscosity, gelation behavior, concentration of initiator and accelerator, *etc.*, must be carefully studied. The idle time, one of the important gelation parameters, is defined as a time length between the addition of the promoting reagents (*i.e.*, initiator and catalysts) and the start of the temperature increase due to exothermic polymerization in the slurry [6,7]. This is the time at which the catalytically treated gelcasting slurry can

*Corresponding author. Tel.: +81 52 735 5256; fax: +81 52 735 5255.
E-mail address: iwa@nitech.ac.jp (S. Iwata).

0272-8842/$ - see front matter © 2012 Elsevier Ltd and Techna Group S.r.l. All rights reserved.
http://dx.doi.org/10.1016/j.ceramint.2012.12.034

be further processed and cast into a mold [8]. The accurate determination of such idle time during the rise in temperature of the polymerizing slurry has been difficult due to the limited accuracy of the temperature sensor, and the gelation behavior of the slurry cannot be determined by that method. An alternative approach to address these problems is to know the profile of the increasing behavior of slurry viscosity versus time during the gelation. There are some reported studies that followed the progress of such a viscosity increase versus time using a stress-controlled rheometer system [9–11]. However, based on these methods, the gelcasting slurry is stressed during testing which may alter the information about the actual in-situ solidification behavior of the slurry. Hence, there is a need to explore other techniques that only moderately disturb the progress of gelation while the slurry viscosity is monitored.

Noninvasive techniques [12,13] are promising tools for observing particle dynamics in relation to the viscosity of a ceramic suspension. These include optical and X-ray visualization techniques. In opaque liquids containing solid particles, the optical method is not preferable because the observation of the particle dynamics is obscured by the liquid itself [14]. An easy alternative to the optical technique is the use of X-rays, such as real-time radiography, but the attenuation properties of the suspension blur the particles to be observed. To circumvent this problem, an X-ray computed tomography scanning technique has been explored because of its technical maturity and compatibility with a vapor–liquid contacting system [15–17]. The images, produced using an X-ray CT, have very high resolutions that produce clear pictures of the particle dynamics in a liquid-based suspension. The X-ray CT involves directing a beam of X-rays at a model object and measuring the intensity of the beam after it passes through to a set of detectors. This generates an image representing one thin segment of the object and the process can be repeated several times to produce a series of images from the object. The set of images can then be combined to provide a three-dimensional representation of the object. Hence, this imaging technique can be potentially applied to view a time-dependent position of any opaque objects in the gelcasting slurry.

The aforementioned imaging techniques usually employ a falling opaque object [18,19] in a suspension to determine its viscosity. The analysis is similar to a falling-ball rheometer based on Stokes' solution of the terminal velocity of a sphere falling in creeping flow through an unbounded, incompressible, Newtonian liquid. Since the gelcasting slurry normally exhibits a non-Newtonian flow, an apparent viscosity of the slurry can be measured as if the slurry were a hypothetically Newtonian fluid [14]. Moreover, the flow behavior of the gelcasting slurry can also be described as a power-law fluid in which the equation for the drag coefficient factor, C_D, is approximated as proposed by some researchers [20–22]. With the use of an X-ray CT scanning system having a higher resolution capability, the accurate determination of the time-dependent position of the falling object through the originally opaque ceramic slurry is made possible. Therefore, in this study, we employed a micro X-ray CT scan system to monitor the settling velocity of a small falling steel ball in a gelcasting slurry during the progress of gelation. The settling velocity of the falling steel ball was determined versus the increasing gelation time and was used to calculate the slurry viscosity using Stokes equation. Accordingly, a plot of the calculated viscosity versus gelling time was made in order to gain insight into the gelation behavior of the slurry. Subsequently, the calculated viscosities were compared and discussed using the measured rheological data obtained from the stress-controlled rheometric analyses.

2. Experimental methods

2.1. Preparation of gelcasting slurry

The gelcasting materials and processing procedure employed in this study were the same as used in our previous report [8]. Table 1 shows a list of gelcasting chemicals and ceramic powder used for the preparation of the gelcasting slurry. The slurry was prepared by ball-milling for 24 h and manually mixed with an initiator (1.03 μL/g) to start the polymerization process. The gelation process was accelerated with the addition of the catalyst (0.17 μL/g), and this additive was manually stirred for 120 s to homogenize the gelcast mixture. Subsequently, the bulk density of the gelcast slurry, ρ, was measured at about 2.50×10^3 kg/m^3.

Table 1
The composition of aqueous gelcasting slurry.

	Agent	Vendor	Conc. (wt%)
Alumina powder	AL160-SG-4 (D_{50}=0.55 μm)	Showa Denko Corp.	80.01
Dispersant	Seruna D-305 (ammonium polyacrylate)	Chukyo Yushi Corp.	0.72
Reactive monomer	Methacrylamide (MAM)	Wako Pure Chemical Co.	3.15
Cross-linker	*N*,*N*′ methylenebis-acrylamide (MABM)	Wako Pure Chemical Co.	1.05
Water	Distilled water		15.07
Initiator	Ammonium peroxodisulfate (10% solution)	Wako Pure Chemical Co.	–
Catalyst	*N*,*N*,*N*′,*N*′-tetramethyl-ethylenediamine	Wako Pure Chemical Co.	–

2.2. Measurement of the slurry viscosity by falling ball velocimetry using the micro X-ray CT scanning system

In this experiment, we measured the actual settling velocity of a small steel ball in the gelcasting slurry. Three steel balls of bearing grade quality were used and each had the same density, ρ_p, of 7.85×10^3 kg/m^3 and diameter, D_p, of 0.500 mm.

Fig. 1 shows the set-up for the experimental apparatus that consisted of a microfocus X-ray CT scanning system (inspeXio SMX-90CT, Shimadzu Co. Ltd., Kyoto, Japan), a sample bottle, computer with monitor, and a high-density video camera. Fig. 2 shows a schematic diagram of the sample bottle used to contain the gelcasting slurry. The inside diameter and height were 40 mm and 120 mm, respectively. Three magnets were respectively used for holding the three steel balls at the top of the sample bottle. When one of the magnets was removed, the corresponding steel ball started to free fall through the slurry. The time interval between ball droppings was determined based on the time it takes for the preceding ball to get closer to the bottom of the sample bottle. To record the ball dropping process, the video data from the monitor attached to the X-ray system was recorded by another computer with the aid of a high-density video camera. The higher frame rate (about 12 fps) of the microfocus X-ray CT scanning system was used throughout the experiments at the resolution mode of 512×512 pixels. The video monitoring of the micro X-ray system was then started 300 s after the addition of the catalyst. X-rays were then emitted from a fixed source. As time elapsed, the distance between the X-ray source and the falling steel ball changed very slightly. Therefore, the coordinates of the falling steel ball were corrected for the size of steel ball and diameter of the sample bottle on the PC monitor. The time elapsed for the falling ball was then determined using a stopwatch program shown on the computer screen. Finally, the settling velocity of the steel ball was evaluated from the stored video data.

The slurry viscosity was calculated using the Stokes equation [20–22]. In this experiment, the generalized Reynolds

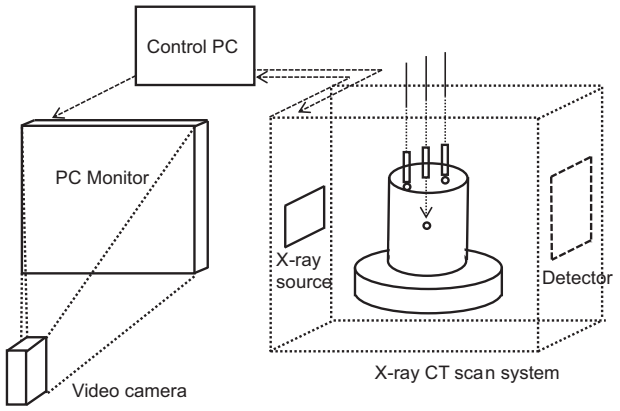

Fig. 1. Experimental set-up of X-ray CT scan system.

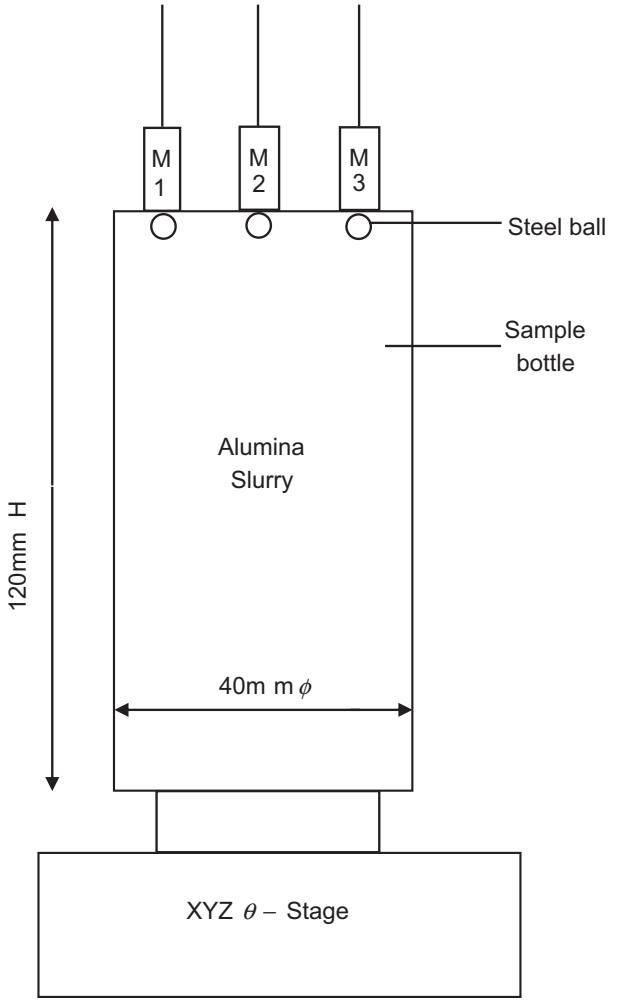

Fig. 2. Schematic diagram of the falling-ball experiment inside a bottle.

number, R_e, was approximated on the order of 10^{-4}. The drag coefficient, C_D, can then be simplified by neglecting the fluid inertia effect as

$$C_D = \frac{24}{R_e}\left(1+\frac{3}{16}R_e\right) \approx \frac{24}{R_e} \tag{1}$$

In this case, the effect of multi-particle hydrodynamic interactions on the friction [16] along the surface of the falling steel ball was negligible because its diameter (D_p=0.5 mm) was much greater than the alumina particles (D_{50}=0.55 μm). Therefore, the slurry viscosity, η can be evaluated from the settling velocity, u, using the Stokes equation,

$$u = \frac{\left(\rho_p-\rho\right)g}{18\eta} D_p{}^2 \tag{2}$$

where g is the acceleration due to gravity.

2.3. Measurement of the slurry viscosity by the rheometer

For a comparative evaluation, we performed strain oscillatory shear experiments using a rheometer (RheoStress 600

system, Haake Corp.). The rheometer was equipped with a parallel plate type sensor with a diameter of 35 mm and a glass enclosure to prevent the slurry from drying out during the measurement. A surface dip treatment was applied to both surfaces of the set of sensors to avoid slipping while the plate gap was kept constant at 1 mm. The progress of gelation was followed in terms of the complex viscosity versus time at a constant frequency of 1 Hz and varying shear strains of 0.1, 0.5, and 1. Finally, the gel point of the gelcasting slurry was also determined by plotting the loss tangent data versus the increasing gelation time subjected to different frequencies.

3. Results and discussion

3.1. Measurement of slurry viscosity by falling ball viscometry

Fig. 3 shows a time series of photographs extracted from the PC video data for the falling steel ball through the slurry in the sample bottle. The falling steel ball can be clearly seen as a black spot at the center of dashed circle on each panel. It was observed that the descending steel ball followed a vertical path indicating that the assumptions of neglecting the wall effect and particle friction were probably satisfied [23,24]. To ensure repeatability of the results, three runs were carried out under videotaped observations. The captured real-time data provided an accurate determination of the time-dependent position of the falling ball for calculating its velocity. Hence, Fig. 4 depicts the settling velocity, u, evaluated from the extracted video data for the three runs. The horizontal axis is the gelation time, t, defined as the elapsed time after the addition of the catalyst. As can be seen from Fig. 4, the settling velocity gradually decreases with the increase in the gelation time. Moreover, the plots of the three runs are smoothly connected, indicating a good reproducibility of the experiments.

Based on the measured settling velocity of the descending ball through the slurry, the slurry viscosity can be calculated using Eq. (2) and the data were plotted on the logarithmic scale shown in Fig. 5. It can be observed that the logarithmic viscosity profile can be divided into three regions. The fitting of a straight line to every region provided three different slopes in an increasing manner. The first region is the plateau of a constant viscosity region that may correspond to the idle

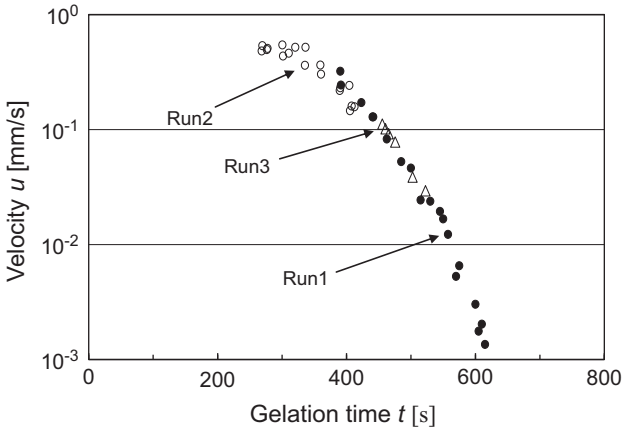

Fig. 4. The velocity of the falling steel ball (D_p=0.500 mm) from three runs.

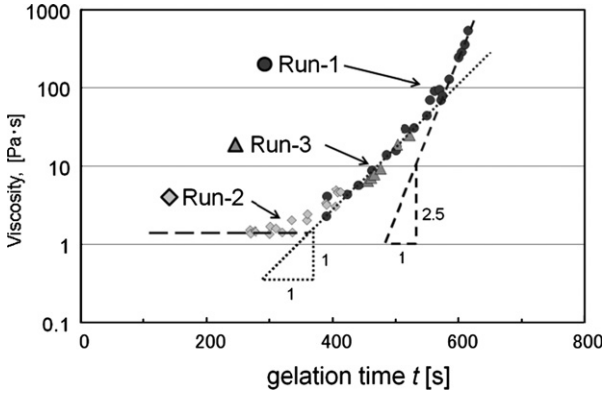

Fig. 5. The calculated viscosity based on the velocity of the falling ball using Stokes law.

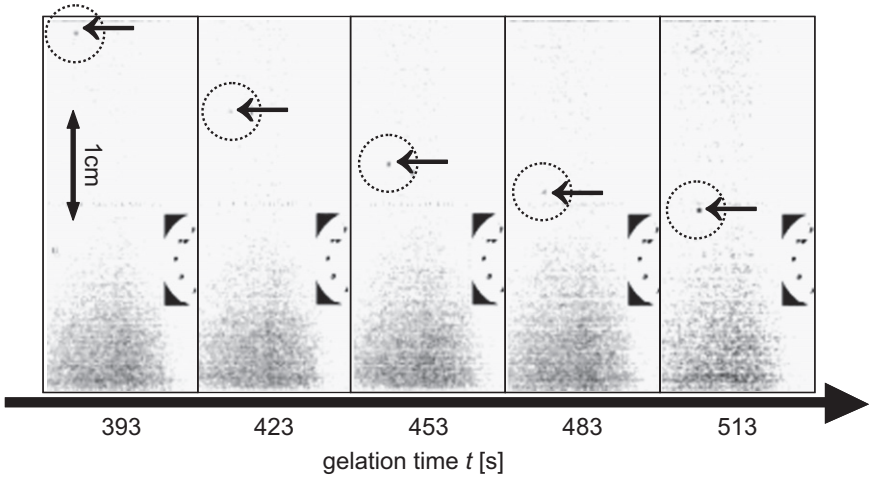

Fig. 3. Series of images of the falling steel ball (D_p=0.500 mm) obtained by the X-ray CT scanning system (RUN1).

time of the slurry. Young et al. [2] showed that the slurry viscosity remains constant during the early stage before the start of the gelation. The intersection [6,9] of the straight lines for regions 1 and 2 may provide a good estimate of such idle time. It can also be deduced that regions 2 and 3 are depicting the progression of the gelation process through polymerization that causes the rise in slurry the viscosity. The evolution of the viscosity increase can be schematically illustrated by the slurry microstructure shown in Fig. 6 as proposed in the present study. During the early stage after casting, the contributing effect to the viscosity is the prevailing bulk viscosity of the slurry as shown in Fig.6(i) when the monomer is not yet reacted or connected. This corresponds to the observed time length (the idle time) of about 300 s, which is represented by the plateau viscosity depicted in Fig. 5. Immediately after the first region, the slurry viscosity began gradually increasing and entered the next region. The second region depicts a gradual increase in the logarithm of the viscosity versus the gelation time. In this region, a small amount of the polymer chains is formed and forms a random network configuration as schematically shown in Fig. 6(ii). After about 550 s, the slope of the fitting line increased again up to about 2.5 times higher than the one in the second region, which may correspond to the increasing formation of the chain entanglements of the polymers as schematically illustrated in Fig. 6(iii). This behavior is demonstrated by region 3 in Fig. 5, which is a consequence of the increasing concentration of the interconnected polymer networks due to the increasing polymerization rate.

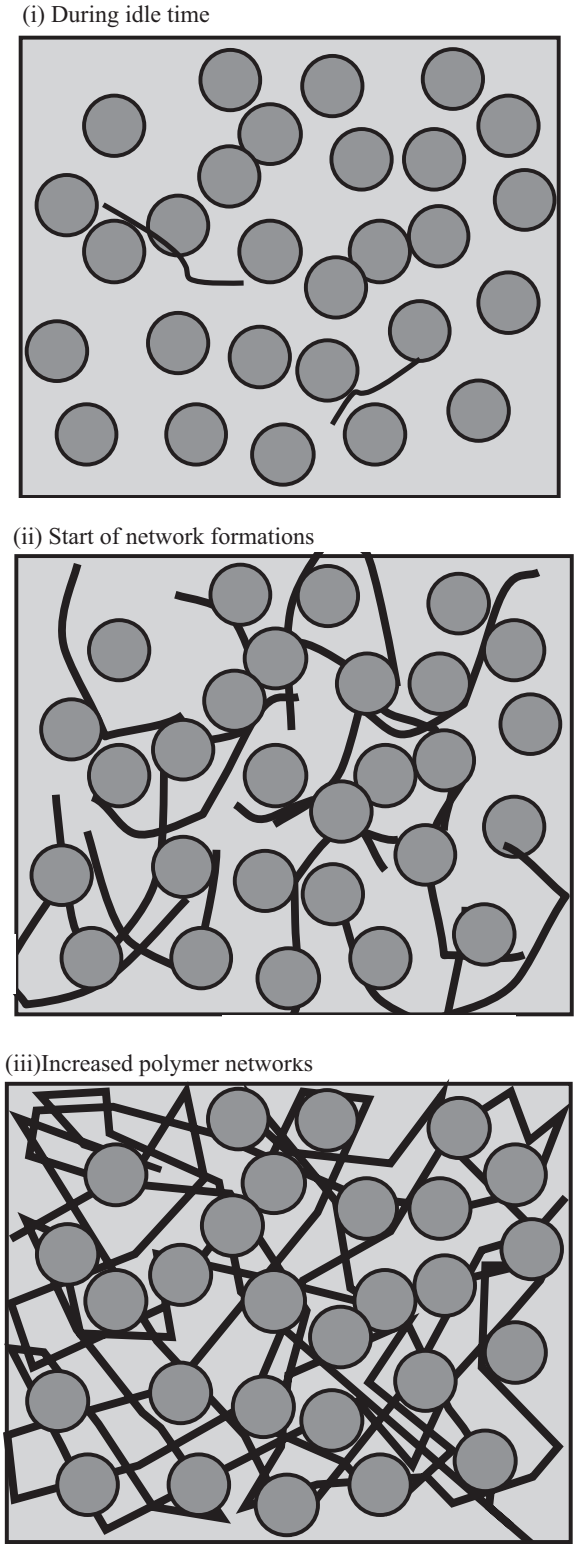

Fig. 6. Proposed schematic evolution of slurry microstructure during in-situ solidification (three stages).

The rate of radical polymerization, r_p, can be expressed as

$$r_p = K[I]^{0.5}[m] \tag{3}$$

where K is the reaction rate constant, $[I]$ is the initiator concentration, and $[m]$ is the monomer concentration [25]. During the initial stage of polymerization, the monomer concentration $[m]$ can be assumed to be constant. If the initiator concentration $[I]$ is considered constant, the polymer concentration $[p]$ is proportional to the gelation time, t, which is expressed as

$$[p] \propto kt \tag{4}$$

where k is the proportionality constant.

It is well known that the viscosities of polymer melts and solutions show a shift with a linear dependence on the product of polymer concentration $[p]$ and molecular weight M_w, (i.e., $[p]M_w$) in the lower value region. However, when the value of the product $[p]M_w$ exceeds a certain level at about 600 s, the dependence of the product will be increased up to 3.4 times longer than the linear dependence case due to the effect of the polymer entanglement [26–28] as represented by Eq. (5).

$$\eta \propto ([p]M_w)^{3.4} \tag{5}$$

As can be seen from Fig. 5, the slope of the line is 2.5, which is slightly lower than the expected power number in Eq. (5). It is postulated that this discrepancy might be due to the polymerization network that is affected by the presence of a large amount of alumina particles.

3.2. Measurement of slurry viscosity and gel point by the rheometer

The graph in Fig. 7 shows the typical dependence of the complex viscosity on time during the gelation process of the gelcast suspension at 25 °C. It was observed that at the constant frequency of 1 Hz, the complex viscosity decreased with the increasing shear strain. This slurry behavior is typical tendency for a non-Newtonian slurry with flow described by the power law model [29]. This effect might be attributed to the disturbance of the applied straining force to the polymerization process. Nevertheless, all the curves exhibited an increasing trend as the gelation time increased.

By observing curves (A), (B), and (C) in Fig. 7, the viscosity trend exhibited only two stages of increasing viscosity. The first stage, which is the idle time, was missing which might be due to large strains imposed on the rheometer at the controlled deformation (CD) and controlled stress (CS). A very small strain oscillation [9,11] might be used on the rheometer to determine it, but it was not pursued because the data were too erratic to provide reasonable information. Instead, an experiment was done using a continuous shear rate (CR) with the steady rate of $50\ s^{-1}$. The resulting viscosity profile is represented by curve (D) in Fig. 7, which exhibited the lowest viscosity resulting from the imposed condition in the continuous rotational mode. This indicated that the measurement of the viscosity under the rotation mode causes considerable destruction of the polymer networks typified by the large decrease in the slurry viscosity. Therefore, measurement by a steady rotation is unsuitable for following the progress of slurry gelation. Nevertheless, it can be observed that there is almost a constant viscosity until about 500 s which could be the idle time. However, such a measured idle time does not reflect the actual in-situ solidification of the gelcasting slurry.

The gel point of the gelcasting slurry was also evaluated in terms of the viscoelastic properties of the gelling slurry. Takahashi [30,31] has suggested a method of gel point determination involving loss tangent curves at different

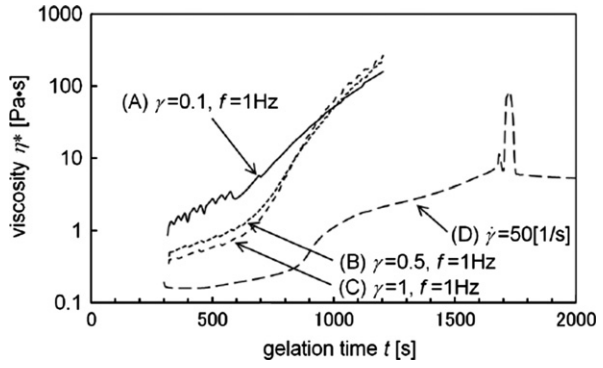

Fig. 7. The complex viscosity of gelcasting slurry in terms of gelation time measured by the rheometer. (A and B obtained at controlled stress (CS); B taken at controlled deformation (CD); and D taken at controlled rate (CR).)

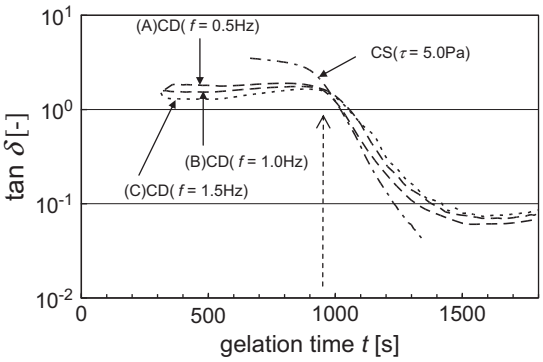

Fig. 8. Loss tangent versus gelation time for gelcasting slurry at different frequencies.

frequencies. These curves are expected to cross at a common gel point, t_c, representing the transition point of the viscous slurry at which the energy dissipation is high during gelation to an elastic solid with a low energy dissipation. Moreover, at the transition point, the loss tangent of the slurry becomes frequency independent that roughly indicates the gelation time [32]. Hence, the experimental curves in Fig. 8 depicted a similar loss tangent ($\tan\delta$) profile versus gelling time for a gelcasting slurry subjected to different frequencies.

It is clearly observed that all the curves revealed a gelling time of 980 s as their common point of intersection. It is worthwhile to point out that the viscous region on the loss tangent curve corresponds to the schematic diagram of the slurry in Fig. 6(ii) whereas the solid-like region is represented by Fig. 6(iii). Moreover, the falling ball method used in the present study is only applicable in the viscous region where the gelcasting slurry has a sufficient fluidity for the ball to descend.

3.3. Comparative evaluation between slurry viscosities measured by the falling ball and the rheometer

The falling ball method presents a potential tool to follow the viscosity increase while the gelcasting slurry is polymerizing. The merit of this method over a viscoelastic study stems from the nonaggressive nature of the test using the X-ray CT scan. Comparing Figs. 5 and 7, it can be deduced that the profile of the logarithm of the measured viscosities of the falling ball method is closer to rheometric studies employing a lower shear strain and frequency during the measurements. However, the rheometric study failed to clearly detect the appropriate length of the idle time. It requires careful implementation of rheological settings during the measurements to provide reproducible results. The detection of the end of the idle time is crucial during the casting step because it provides allowance for further processing steps such as mixing of the additives, degassing, and casting operation. The falling ball method was found to be quite sensitive and convenient in exactly detecting the end of the idle time as compared to the

rheometric experiment. This is may be because the falling ball method allows the network structure of the polymer to smoothly grow without much disturbance. As the steel ball enters the growing network structure of the polymer, it slowly breaks the polymerizing structure while descending at a low speed. Therefore, the actual evolution of the viscosity increase during in-situ solidification is clearly observed. In the present experiment, the falling ball method detects the starting increase in the slurry viscosity after 350 s whereas the rheometric study detects it at about 500 s. It is also noted that the viscosity obtained by the rheometric study is lower than the falling ball during the method at earlier stage of the reaction. This is maybe because the applied shear strain in the rheometric experiment reduces the growth of the network structure during polymerization as the slurry is continuously disturbed in an aggressive manner [33].

Knowledge of the viscosity profile for a given gelcasting slurry is indeed important during the processing of additives and subsequent casting of the slurry into a mold. If the casting operation is done to efficiently fill the slurry in the mold, the slurry must have a sufficient fluidity as schematically illustrated in Fig. 6(i) and then gelation can be allowed to proceed in order to solidify the slurry in a homogeneous manner. In contrast, if the casting operation is done when the slurry is under the condition specified by Fig. 6(ii) or (iii), mold filling is difficult to achieve as the developing polymer networks are disturbed under shear flow. As a consequence, the gelled ceramic body possesses nonuniform distributions of the polymerized structure while introducing high stresses to the freshly gelled body. The stressed body ultimately develops serious cracks during the drying and sintering steps. Therefore, sensitive monitoring of the viscosity increase is required for a particular gelcasting mixture which could be provided by the falling ball method.

4. Conclusion

A micro X-ray CT scan system was successfully employed to monitor the settling velocity of the small falling steel ball in the gelcasting slurry during the progress of in-situ gelation. The falling ball method sensitively detected the start of gelation of the gelcasting slurry at an earlier time as compared to the rheometric study. Such determination of the gelling time under stress conditions overestimates the time of gelation because the polymer networks are disrupted thus leading to a low viscosity slurry. The measured viscosity by the falling ball method is only closer to the one obtained by the rheometric experiment under stress-controlled conditions involving a lower strain and frequency. The profile of the logarithm of the calculated viscosities based on the velocity of the steel ball was found to be classified into three regions having increasing slopes. These regions described the gradual progression of the gelling slurry from a highly fluid state to a solid-like behavior due to the increasing concentration of the polymerized networks.

References

[1] O.O. Omatete, M.A. Janney, R.A. Strehlow, Gelcasting – A new ceramic forming process, Journal of American Ceramic Society Bulletin 70 (1991) 1641–1649.
[2] A.C. Young, O.O. Omatete, M.A. Janney, P.A. Menchhofer, Gelcasting of alumina, Journal of American Ceramic Society 74 (1991) 612–618.
[3] M.A. Janney, W. Ren, G.H. Kirby, S.D. Nunn, S. Viswanathan, Gelcast tooling: net shape casting and green machining, Materials and Manufacturing Processes 13 (1998) 389–403.
[4] M.A. Janney, O.O. Omatete, C.A. Walls, S.D. Nunn, R.J. Ogle, G. Westmoreland, Development of low-toxicity gelcasting systems, Journal of American Ceramic Society 81 (1998) 581–591.
[5] K. Niihara, B. Kim, T. Nakayama, T. Kusunose, T. Nomoto, A. Hikasa, T. Sekino, Fabrication of complex-shaped alumina/nickel nanocomposites by gelcasting process, Journal of European Ceramic Society 24 (2004) 3419–3425.
[6] P. Sepulveda, J.G.P. Binner, Persulfate-amine initiation systems for gelcasting of ceramic foams, Chemistry of Materials 13 (2001) 4065–4070.
[7] P. Sepulveda, J.G.P. Binner, Evaluation of the in situ polymerization kinetics for the gelcasting of foams, Chemistry of Materials 13 (2001) 3882–3887.
[8] T. Kato, T. Shirai, H. Watanabe, M. Fuji, M. Takahashi, Y. Yamada, S. Iwata, Y. Kato, H. Mori, Effect of mixing condition of additives on the solidification of green body by gelcasting method, Journal of Ceramic Society of Japan 117 (2009) 987–991.
[9] O. Bera, M. Trunec, Optimization of fine alumina gelcasting using in situ dynamic rheology, Journal of American Ceramic Society 95 (2012) 2849–2856.
[10] D. Calvet, J.Y. Wong, S. Giasson, Rheological monitoring of polyacrylamide gelation: importance of cross-link density and temperature, Macromolecules 37 (2004) 7762–7771.
[11] T. Savart, C. Dove, B.J. Love, In situ dynamic rheology study of polyacrylamide during gelation coupled with mathematical models of viscosity advancement, Macromolecular Materials and Engineering 295 (2010) 146–152.
[12] J. Chaouki, F. Larachi, M.P. Dudukovic, Noninvasive tomographic and velocimetric monitoring of multiphase flows, Industrial and Engineering Chemistry Research 36 (1997) 4476–4503.
[13] F.J. Dickin, R.A. Williams, M.S. Beck, Determination of composition and motion of multicomponent mixtures in process vessels using electrical impedance tomography. I. Principles and process engineering applications, Chemical Engineering Science 48 (1993) 1883–1897.
[14] L.A. Mondy, A.L. Graham, A. Majumdar, L.E. Bryant Jr., Techniques of measuring particle motions in concentrated suspensions, International Journal of Multiphase Flow 12 (1986) 497–502.
[15] C.E. Schmit, D.B. Carmel, R.B. Eldridge, The experimental application of X-ray tomography to a vapor–liquid contactor, Chemical Engineering Science 56 (2001) 3431–3441.
[16] X. Lu, P. Miao, A.T. Watson, G.P. Pepin, R.M. Moss, L. Semmelbeck, X-ray computed tomography studies of gas storage and transport in Devonian shales, AIChE Journal 40 (1994) 1246–1253.
[17] M. Bieberle, F. Barthel, H. Menz, H. Mayer, U. Hampel, Ultrafast three-dimensional X-ray computed tomography, Applied Physics Letters 98 (2011) 034101.
[18] Y.I. Cho, J.P. Hartnett, W.Y. Lee, Non-Newtonian viscosity measurements in the intermediate shear rate range with the falling-ball viscometer, Journal of Non-Newtonian Fluid Mechanics 15 (1984) 61–74.
[19] I. Machac, I. Ulbrichova, T.P. Elson, D.J. Cheesman, Fall of spherical particles through non-Newtonian suspensions, Chemical Engineering Science 50 (1995) 3323–3327.

[20] K. Kubo, E. Mito, Y. Nakagawa, M. Hayakawa, Powder, Theory and Applications, Maruzen (Tokyo), 1962, pp. 317–319.
[21] R.P. Chhabra, Second edition, Bubbles, Drops, and Particles in Non-Newtonian Fluids. CRC Press (Boca Raton), 2006, pp. 49–122.
[22] H. Yanagida, Engineering System for Fine Particles, Fuji Techno system (Tokyo), I, (2001) 205–206.
[23] D.D. Joseph, Y.J. Liu, M. Poletto, J. Feng, Aggregation and dispersion of spheres falling in viscoelastic liquids, Journal of Non-Newtonian Fluid Mechanics 54 (1994) 45–86.
[24] A.E. Kaiser, A.L. Graham, L.A. Mondy, Non-Newtonian wall effects in concentrated suspensions, Journal of Non-Newtonian Fluid Mechanics 116 (2004) 479–488.
[25] S. Okamura, A. Nakajima, S. Onogi, H. Kawai, Y. Nishijima, T. Higashimura, N. Ise, Introduction to Polymer, Kagaku Dojin (Kyoto), 1981, pp. 218–243.
[26] G. Berry, T. Fox, Advances in Polymer Science 5 (1968) 261–357.
[27] P.J. Carreau, D.C.R. De Kee, R.P. Chhabra, Rheology of Polymeric Systems, Hanser Gardner Publications, Inc., 1997, pp. 50–57.
[28] S. Onogi, Rheology for Chemists, Kagaku Dojin (Kyoto), 2000, pp. 150–152.
[29] Z. Chen, P. Chao, S. Chiu, Empirical viscosity model for polymers with power-law flow behavior, Journal of Applied Polymer Science 88 (2003) 3045–3057.
[30] M. Takahashi, Journal—Society of Rubber Industry Japan 66 (1993) 237–244.
[31] B. Chiou, S.R. Raghavan, S.A. Khan, Effect of colloidal fillers on the cross-linking of a UV-curable polymer: gel point rheology and the Winter–Chambon criterion, Macromolecules 34 (2001) 4526–4533.
[32] Y. Jiao, D. Gyawali, J.M. Stark, P. Akcora, P. Nair, R.T. Tran, J. Yang, A rheological study of biodegradable injectable PEGMC/HA composite scaffolds, Soft Matter 8 (2012) 1499–1507.
[33] J.A. Martins, W. Zhang, A.M. Brito, Saturation of shear-induced isothermal crystallization of polymers at the steady state and the entanglement–disentanglement transition, Macromolecules 39 (2006) 7626–7634.